Hydrophobic Core Substitutions in Calbindin D_{9k}: Effects on Ca^{2+} Binding and Dissociation†

Birthe B. Kragelund,‡ Malin Jönsson,‡ Giuseppe Bifulco,§,|| Walter J. Chazin,§ Hanna Nilsson,‡ Bryan E. Finn,*,‡ and Sara Linse*,‡

Physical Chemistry 2, Lund University, Chemical Centre, P.O. Box 124, S-221 00 Lund, Sweden, and Department of Molecular Biology, Research Institute of Scripps Clinic, La Jolla, California 92037

Received October 24, 1997; Revised Manuscript Received March 13, 1998

ABSTRACT: Hydrophobic core residues have a marked influence on the Ca^{2+}-binding properties of calbindin D_{9k}, even though there are no direct contacts between these residues and the bound Ca^{2+} ions. Eleven different mutants with substitutions in the hydrophobic core were produced, and their equilibrium Ca^{2+}-binding constants measured from Ca^{2+} titrations in the presence of chromophoric chelators. The Ca^{2+}-dissociation rate constants were estimated from Ca^{2+} titrations followed by ^1H NMR[1] and were measured more accurately using stopped-flow fluorescence. The parameters were measured at four KCl concentrations to assess the salt dependence of the perturbations. The high similarity between the NMR spectra of mutants and wild-type calbindin D_{9k} suggests that the structure is largely unperturbed by the substitutions. More detailed NMR investigations of the mutant in which Val61 is substituted by Ala showed that the mutation causes only very minimal perturbations in the immediate vicinity of residue 61. Substitutions of alanines or glycines for bulky residues in the center of the core were found to have significant effects on both Ca^{2+} affinity and dissociation rates. These substitutions caused a reduction in affinity and an increase in off-rate. Small effects, both increases and decreases, were observed for substitutions involving residues far from the Ca^{2+} sites and toward the outer part of the hydrophobic core. The mutant with the substitution Phe66 → Trp behaved differently from all other mutants, and displayed a 25-fold increase in overall affinity of binding two Ca^{2+} ions and a 6-fold reduction in calcium dissociation rate. A strong correlation ($R = 0.94$) was found between the observed Ca^{2+}-dissociation rates and affinities, as well as between the salt dependence of the off-rate and the distance to the nearest Ca^{2+}-coordinating atom. There was also a strong correlation ($R = 0.95$) between the Ca^{2+} affinity and stability of the Ca^{2+} state and a correlation ($R = 0.69$) between the Ca^{2+} affinity and stability of the apo state, as calculated from the results in the present and preceding paper in this issue [Julenius, K., Thulin, E., Linse, S., and Finn, B. E. (1998) *Biochemistry* 37, 8915−8925]. The change in salt dependencies of k_{off} and cooperativity were most pronounced for residues completely buried in the core of the protein (solvent accessible surface area ≈ 0). Altogether, the results suggest that the hydrophobic core residues promote Ca^{2+} binding both by contributing to the preformation of the Ca^{2+} sites in the apo state and by preferentially stabilizing the Ca^{2+}-bound state.

Hydrophobic residues interact more favorably with each other than with solvent water. Consequently, the hydrophobic side chains are packed into one or more clusters, or hydrophobic cores, in a folded protein. A large fraction of the hydrophobic side chains is thus found in the interior of the protein and often would not seem to participate directly in mediating the functions of the protein, which generally occur at or near the protein surface. However, functional properties such as ligand binding and enzyme catalysis can be modulated by many different factors, not only local interactions between a ligand and its binding site. Thus, the observed ligand-binding affinity is often the net result of a large number of contributions stemming from essentially the entire protein molecule or large portions thereof.

The activation of an EF-hand protein by binding of Ca^{2+} ions represents a typical example where the relationship between function and packing can be explored. Among the

† This work was supported by The Swedish Natural Science Research Foundation (grant K 10178-305 S.L.), National Institutes of Health (Grants GM 40120 to W.J.C. and GM 14691 to B.E.F.), the Carlsberg Foundation (B.B.K.). W.J.C. is a Faculty Research Fellow of the American Cancer Society (FRA-436).

* Address correspondence to this author. E-mail: sara@bor.fkem2.lth.se.

‡ Lund University.

§ Research Institute of Scripps Clinic.

|| Present address: Dipartimento di Scienze Farmaceutiche, Universita di Salerno, P.zza Vittorio Emanuele 9, 84084 Penta (SA) Italy.

[1] Abbreviations: NMR, nuclear magnetic resonance; EDTA, ethylendiaminetetraacetic acid; Tris, tris(hydroxymethyl)aminomethane; SDS, sodium dodecyl sulfate; Quin 2,2-[[bis[(carboxymethyl)amino]-5-methylphenoxy]-methyl]-6-methoxy-8-[bis(carboxymethyl)amino]-quinoline; 5,5′Br_2-BAPTA, 5,5′-dibromo-1,2-bis(*o*-aminophenoxy)-ethane-*N*,*N*,*N*′,*N*′-tetraacetic acid; COSY, J-correlated spectroscopy; NOESY, nuclear overhauser enhancement spectroscopy; TOCSY, total correlation spectroscopy; DIPSI, decoupling in the presence of scalar interactions; HE, Hahn-echo; 2Q, double quantum spectroscopy; P43M, calbindin D_{9k} mutant with the substitution Pro43 → Met. All other mutants contain the Pro43 → Met substitution plus the substitutions as follows: L6V, Leu6 → Val; F10A, Phe10 → Ala; L23A, Leu23 → Ala; L23G, Leu23 → Gly; L28A, Leu28 → Ala; V61A, Val61 → Ala; V61G, Val61 → Gly; F66A, Phe66 → Ala; F66W, Phe66 → Trp; V70L, Val70 → Leu; I73V, Ile73 → Val.

S0006-2960(97)02643-3 CCC: $15.00
Published on Web 05/29/1998

factors that govern the Ca^{2+} affinity of a protein, there are of course essential contributions from the backbone and side-chain oxygen atoms that directly coordinate the metal ion, as well as from side chains that stabilize Ca^{2+}-coordinating water molecules. In many cases, a drop in affinity has been observed when an existing site is perturbed by altering one or more of these side chains. For example, when the two most highly conserved calcium coordinating residues in the EF-hand sites are altered, there is a large drop in affinity (*2*, *3*). The affinity is also depedent on the exact positioning of charged coordinating groups (*4*). However, the collective picture emerging from crystallographic analysis of a large number of calcium-binding proteins fails to show any significant correlation between Ca^{2+} affinity and factors such as the number of coordinating oxygens provided by the protein, the number of coordinating water molecules, net negative charge on the coordinating oxygens, or the number of coordinating backbone oxygens (*5*).

Contributions from regions outside the binding site must have a large influence on the Ca^{2+} affinity. Factors that promote the correct fold of the binding site will contribute via "preformation" of the site, analogous with the macrocycle effect observed for small organic chelates (*6*). Factors which facilitate conformational changes upon Ca^{2+} binding will lead to higher affinity (*7*, *8*), whereas factors opposing this change will lead to reduced affinity (*9*, *10*). The long-ranged nature of electrostatic forces means that charged residues up to approximately 15 Å from the binding site will contribute to the affinity for ionic ligands (*11*−*13*). Significant contributions to the affinity arise also from solvent effects such as pH (*14*), temperature (*14*, *15*), electrolyte composition (*12*, *16*), and protein concentration (*17*). In addition, by thermodynamic arguments, if the protein interacts with another protein in a Ca^{2+}-dependent manner, the presence of that protein will also increase the Ca^{2+} affinity.

The strong driving force for the hydrophobic packing of the EF-hand motif has been clearly demonstrated in experiments using isolated EF-hands, for example from troponin C (*18*, *19*), calmodulin (*20*), and calbindin D_{9k} (*21*, *22*). These fragments, which literally contain only one-half of the hydrophobic core, are observed to form homodimers in the presence of Ca^{2+}. When such a homodimer is mixed with its natural partner, the heterodimer is preferentially formed at the expense of the homodimers. These observations suggest a very high specificity in the packing of the hydrophobic core, which involves a large hydrophobic contact area between the two EF-hands. A strong preference for the native arrangement of subdomains has also been found for parvalbumin (*23*) and the sarcoplasmic calcium-binding protein (*24*).

The aim of the present work is to evaluate to what extent the Ca^{2+}-binding properties of a small globular protein is dependent on interactions within the hydrophobic core. We have therefore studied the effects on the Ca^{2+} affinity and Ca^{2+}-dissociation rate of calbindin D_{9k}, upon mutation of residues that are present in the protein core both in the Ca^{2+}-free (apo) and bound forms. Calbindin D_{9k} is one of the smallest members of the calmodulin superfamily of EF-hand proteins. It contains only two EF-hands and binds two Ca^{2+} ions with high affinity and positive cooperativity (*12*). Its structure is known to high resolution in both crystal (Ca^{2+} loaded, refs *25*, *26*) and solution (Ca^{2+} loaded, ref *27*; apo, ref *28*) and shows that the hydrophobic residues form a tightly packed core with no significant hydrophobic patches on the protein surface. The approximate dimensions of the protein are 25 × 30 × 30 Å. The two EF-hands interact via a large hydrophobic contact area with global dimensions of ca. 20 × 25 Å and via two cross strand hydrogen bonds linking the Ca^{2+}-binding loops. The conformational response to Ca^{2+} binding is much smaller than for the globular domains of calmodulin and troponin C, and the process does not appear to lead to any overall change in exposure of hydrophobic residues (*28*, *29*).

Eleven calbindin D_{9k} mutants with substitutions of hydrophobic residues scattered throughout the core have been produced. Equilibrium Ca^{2+}-binding constants have been measured from titrations in the presence of a competitive chromophoric chelator at four KCl concentrations. The Ca^{2+}-binding process has been followed by ^{1}H NMR, and the Ca^{2+}-dissociation rates have been measured by stopped-flow fluorescence also at four KCl concentrations. The overall structural integrity of the proteins have been compared by one-dimensional NMR. More in-depth ^{1}H NMR analyses have been carried out for one mutant containing a substitution in the cross-strand β-type interaction linking the two Ca^{2+} sites, and whose side chain is also part of the hydrophobic core. These results are discussed in terms of the relationship between the Ca^{2+}-binding function and interior packing of the protein.

MATERIALS AND METHODS

Proteins. All calbindin D_{9k} mutants were expressed in *Escherichia coli* from synthetic genes and purified as described previously (*30*). The purity was confirmed by agarose gel electrophoresis in the presence of 1 mM EDTA or 2 mM $CaCl_2$, SDS polyacrylamide gel electrophoresis, isoelectric focusing, and ^{1}H NMR. The residual calcium content was measured from titrations in the presence of Quin 2 and was in all cases below 0.1 equiv.

Chemicals. Quin 2 was purchased from Fluka (Buchs, Switzerland), and 5,5′-Br_2-BAPTA from Molecular Probes (Eugene, Oregon). All other chemicals were of highest grade commercially available. The buffer was prepared and stored with Chelex-100 (Bio/Rad) in a dialysis bag in the container to keep the free calcium concentration at a minimum.

Chelator Method. The macroscopic calcium-binding constants were determined from titrations in the presence of a chromophoric chelator as described (*12*, *22*). The titrations were made in 2 mM Tris/HCl, pH 7.5, at four salt concentrations (no KCl added, 10 mM KCl, 50 mM KCl, and 150 mM KCl). Three repeat titrations were performed for each case.

^{1}H NMR Titrations. One-dimensional ^{1}H NMR spectra were recorded for 1 mM protein on a GE-Omega spectrometer operating at 500.11 MHz, at 27 °C. The protein was dissolved in H_2O (with 10% D_2O) without the addition of salt, and the pH was adjusted to 7.0 with NaOH or HCl. For the titrations, Ca^{2+} was added in steps of 0.15−0.2 equiv from a stock $CaCl_2$ solution.

Two-Dimensional ^{1}H NMR. 2D NMR experiments were acquired on a Bruker AMX-500 spectrometer at 27 °C. Spectra were referenced to the residual H_2O or HOD resonance at 4.75 ppm. COSY (*31*), 2Q (*32*), and NOESY

(*33*) spectra were acquired using standard phase cycling. A composite 180° pulse (*34*) was used in the middle of the preparation period of the 2Q experiments. TOCSY (*32*) experiments using a DIPSI-2 sequence (*35*) for isotropic mixing were recorded with the modification described by Rance (*36*). NOESY and TOCSY experiments were recorded with sine modulation in t_1 (*37*) and with a Hahn-echo (HE) period after the read pulse in order to improve the baseline (*38*, *39*). Low-power irradiation of the solvent resonance was used during the relaxation delays of 1.2−2.0 s, and during the mixing time of the NOESY experiments.

For assignments of apo V61A, a COSY, two HE-TOCSY (t_m = 60 and 100 ms), and a HE-NOESY (t_m = 200 ms) spectrum were acquired from a 90% ^1H_2O/10% ^2H_2O solution, and 2Q (t_e = 30 ms) was acquired from ^2H_2O solution. Assignments of the $(Ca^{2+})_2$ state were made using COSY, 2Q (t_e = 30 ms), two HE-TOCSY (t_m = 60 and 100 ms), HE-NOESY (t_m = 120 ms), and JR-NOESY (t_m = 200 ms) spectra acquired from a 90% ^1H_2O/10% ^2H_2O solution, and COSY, 2Q (t_e = 30 ms), two HE-TOCSY spectra (t_m = 70 and 100 ms), and HE-NOESY (t_m = 120 ms) spectra acquired in ^2H_2O. For semiquantitative analysis of amide proton exchange, a 1D spectrum was acquired 11 min after dissolving in ^2H_2O, followed by a quick (3 h) 2Q experiment with extensive folding in ω_1, another 1D after 3 h 15 min, a full (18.5 h) 2Q experiment after 3 h 20 min, and a final full 2Q after 24 h. For the $(Ca^{2+})_2$ state, the time points were 11 min, 3 h, and 19 h, and the final 2D experiment was a COSY rather than 2Q spectrum.

Stopped-Flow Studies. Stopped-flow experiments were performed at 299 K using a Biologic SFM3 module connected to a Biologic MOS-200 optical system as light source. The light was led to the cuvette through an optical fiber (Fiberguide Industries). The total fluorescence from excitation at 339 nm was detected by a Hamamatsu R-376 photomultiplier connected to a Biologic PMS200 photomultiplier detection unit. A 2 × 2 mm quartz cuvette was used, and a cut-off filter blocking transmission below 400 nm was inserted in front of the photomultiplier. All solutions were made in 2 mM Tris/HCl, pH 7.5. The proteins were dissolved to a concentration of 15 μM with 40 μM $CaCl_2$, at four different concentrations of KCl, ≤2, 10, 50, and 150 mM. The protein solutions were mixed 1:10 with 20 μM Quin 2, resulting in final reaction conditions of 1.36 μM protein, 3.6 μM $CaCl_2$, and 18 μM Quin 2. Kinetic traces were fitted to single or double exponentials using the program CANOO (Christian Rischel, unpublished results) with linear correction for Quin 2 photo bleaching, providing uncertainties of the fits. The salt dependencies were determined from the linear relationship of the off-rates to the square of the concentration of added potassium chloride.

Calculations of the Distance to the Nearest Calcium-Coordinating Atom. From each of the two calcium-binding loops, six atoms known to be involved in calcium coordination were selected. These atoms were, for site I, A14O, E17O, D19O, Q22O, E27OE1, and E27OE2 and, for site II, D54OD1, D56OD1, D58OD1, E60O, E65OE1, and E65OE2 (*25*, *26*). The distances to all atoms were calculated for both the apo and calcium forms (pdb accession codes 1clb and 2bcb) using the program EXCEL. The Ca^{2+}-loaded form is represented by a set of NMR structures, and the distances here are reported for the first model. The distance deviations among the structures were generally less than 1 Å.

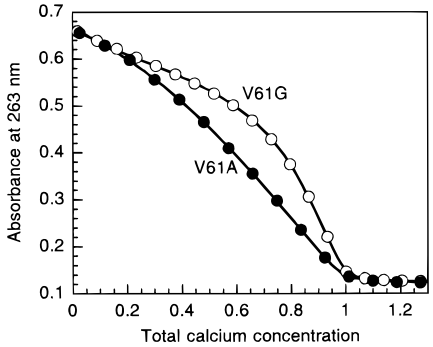

FIGURE 1: Ca^{2+} titrations of 5,5′-Br_2BAPTA in the presence of V61A and V61G at low ionic strength. Absorbance at 263 nm as a function of total Ca^{2+} concentration. Experimental points for V61A (●) and V61G (○). The solid lines are curves obtained by least-squares fitting to the data points as described (*12*). The protein and chelator concentrations were close to 25 μM. The data and curves are normalized such that Ca_{tot} = 1.0 cooresponds to the chelator concentration plus two times the protein concentration.

RESULTS

Design of Mutants Proteins. The mutations were designed to cause changes in side-chain volume of residues that contribute to the hydrophobic core of calbindin D_{9k}. The positions were chosen so as to represent both side chains that are deeply buried in the core or closer to the protein surface. The substituted residues can be roughly grouped into three categories: (i) the two residues that form backbone hydrogen bonds between the two Ca^{2+}-binding loops (Leu23 and Val61) which probe direct coupling between hydrophobic packing and the binding loops, (ii) residues present in the center of the core (Phe10, Leu28, and Phe66) which probe the effect of central core disruptions, and (iii) residues that are at the opposite end of the protein from the Ca^{2+} sites (Leu6, Val70, Ile73) which probe the distance dependence of influences on the Ca^{2+} sites, and Ca^{2+}-induced conformational changes in helix IV (Val70 and Ile73). The notation with one-letter amino acid code is used to refer to the mutants throughout the text. This notation points to the hydrophobic core substitution only, although all mutants have the Pro43 substituted to Met to avoid complications of the cis−trans isomerization of Pro43 as observed in the native protein (*40*). The mutant with the single substitution Pro43 → Met is denoted P43M, and it is used as a reference for the results of the other mutants. The substituted side chains are visualized in Figure 1 of the preceding paper in this issue (*1*).

Equilibrium Ca^{2+}-Binding Constants. The two macroscopic Ca^{2+}-binding constants, K_1 and K_2, were measured for each mutant at four different KCl concentrations from titrations in the presence of a competitive chromophoric chelator (Quin 2 or 5,5′-Br_2−BAPTA depending on the magnitude of K_1 and K_2). Examples of titration curves are shown in Figure 1 for the two mutants V61A and V61G. The resulting Ca^{2+}-binding constants are summarized in Table 1. Each reported value is the mean of three independent experiments. The total free energy change of binding two Ca^{2+} ions was calculated from the macroscopic Ca^{2+}-binding constants as $\Delta G_{tot} = -RT \ln(K_1K_2)$.

Table 1: Macroscopic Calcium-Binding Constants K_1 and K_2

	[KCl]/mM	log K_1	log K_2	$-\Delta G_{tot}$	$-\Delta\Delta G_{\eta=1}$
P43M	≤2	7.75	8.59	93.3	8.2
L6V	≤2	8.22	8.56	95.4	5.7
F10A	≤2	6.84	7.27	80.5	5.9
L23A	≤2	6.96	7.98	85.3	9.2
L23G	≤2	6.59	6.51	74.7	3.0
L28A	≤2	7.44	6.97	82.2	0.8
V61A	≤2	7.77	7.05	84.5	−0.7
V61G	≤2	6.77	8.47	86.9	13
F66A	≤2	7.06	7.88	85.2	8.1
F66W	≤2	8.72	9.02	101.2	4.8
V70L	≤2	8.07	8.00	91.7	3.1
I73V	≤2	7.96	8.72	95.2	7.8
P43M	10	7.17	8.04	86.8	8.4
L6V	10	7.78	8.02	90.1	4.8
F10A	10	6.40	7.10	77.0	7.4
L23A	10	6.50	7.63	80.7	9.9
L23G	10	5.96	6.30	69.9	5.4
L28A	10	6.65	6.69	76.1	3.6
V61A	10	7.12	6.66	78.6	0.8
V61G	10	6.35	8.00	82.0	13
F66A	10	6.68	7.63	81.6	8.8
F66W	10	8.27	8.39	95.1	4.1
V70L	10	7.49	7.50	85.6	4.5
I73V	10	7.50	8.02	88.5	6.4
P43M	50	6.44	7.11	77.4	7.3
L6V	50	6.98	7.11	80.4	4.2
F10A	50	5.84	6.46	70.1	7.0
L23A	50	5.69	7.17	73.4	11.9
L23G	50	5.20	6.09	64.4	8.5
L28A	50	5.86	6.14	68.5	5.0
V61A	50	6.31	5.99	70.2	1.6
V61G	50	5.5	7.3	73.6	14
F66A	50	5.8	7.2	74.1	10.6
F66W	50	7.46	7.35	89.5	3.8
V70L	50	6.64	6.68	75.9	3.6
I73V	50	6.86	7.20	80.2	5.3
P43M	150	5.98	6.50	71.4	6.4
L6V	150	6.48	6.50	74.1	3.6
F10A	150	5.44	5.91	64.8	6.0
L23A	150	5.1	6.8	68.0	13
L23G	150	4.73	5.80	60.1	9.5
L28A	150	5.36	5.70	63.1	5.4
V61A	150	5.83	5.59	65.2	2.1
V61G	150	5.0	7.0	68.7	15
F66A	150	5.54	6.61	69.3	9.5
F66W	150	6.95	6.87	78.9	3.0
V70L	150	6.10	6.14	69.9	3.7
I73V	150	6.31	6.50	73.1	4.5

It is evident that all the examined substitutions of hydrophobic core residues perturb the Ca^{2+}-binding properties. At all four salt concentrations, the effects on the overall affinity, $\Delta G_{tot} = -RT \ln(K_1K_2)$, are rather small for the more distant residues (Figure 2A), whereas reduction in side-chain volume of residues in the center of the core leads to a larger reduction of the Ca^{2+} affinity, especially in the case of F10A and L28A (Figure 2B). The increase in side-chain volume of residue 66 as in F66W leads to a remarkable increase in Ca^{2+} affinity. Substitution of the side chains of the β-sheet residues with smaller ones (glycine or alanine) leads to substantial reductions in Ca^{2+} affinity (Figure 2C). The largest drop in affinity is observed for L23G; the overall affinity for this mutant is 100−1000-fold lower than for P43M depending on KCl concentration. For one of the residues (Val61), the results are somewhat unexpected in that the Val → Ala substitution has a more dramatic effect on the Ca^{2+} affinity than the Val → Gly substitution. The effect of added salt on the overall affinity is the same for P43M, L6V, F66W, V70L, and I73V (21−22 kJ mol^{-1}, comparing low salt and 0.15 M KCl), slightly reduced for L28A, V61A, and V61G (18−19 kJ mol^{-1}), and significantly smaller for F10A, L23A, L23G, and F66A (15−17 kJ mol^{-1}).

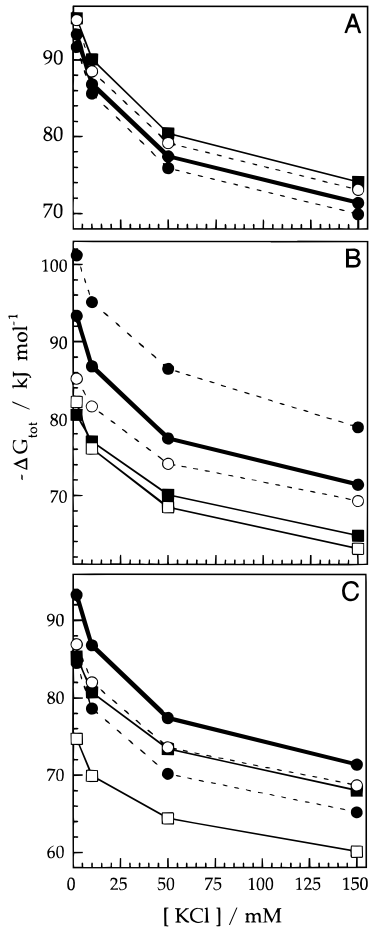

FIGURE 2: Free energy of binding two Ca^{2+} ions, $\Delta G_{tot} = -RT \ln(K_1K_2)$ as a function of salt concentration. The data for the wild-type substitute P43M is shown in all panels (●, solid line). (A) Mutant proteins with substituted residues distant from the Ca^{2+} sites: L6V (■, solid line), V70L (●, dashed line), I73V (○, dashed line). (B) Mutant proteins with substituted residues in the center of the core: F10A (■, solid line), L28A (□, solid line), F66A (○, dashed line), F66W (●, dashed line). (C) Mutant proteins with substituted residues having side chains in the core and involved in the backbone-backbone β-type interaction between the Ca^{2+} sites: L23A (■, solid line), L23G (□, solid line), V61A (●, dashed line), V61G (○, dashed line).

The cooperativity of Ca^{2+} binding is related to the free energy of interaction between the sites, $\Delta\Delta G$, which is negative for positive cooperativity. This parameter is defined as

$$\Delta\Delta G = -RT \ln(K_{II,I}/K_{II}) \quad (1)$$

with the microscopic-binding constants, $K_{II,I}/K_{II}$, defined in Figure 3.

A lower limit to $-\Delta\Delta G$ can be derived from the macroscopic binding constants as

$$-\Delta\Delta G_{\eta=1} = RT \ln(4K_2/K_1) \quad (2)$$

and this lower limit, $-\Delta\Delta G_{\eta=1}$, is identical to $-\Delta\Delta G$ if the two sites have identical affinities, i.e., the ratio $K_{II}/K_I = \eta = 1$. The parameter $-\Delta\Delta G_{\eta=1}$ is inherently less well determined than ΔG_{tot}, especially at high levels of cooper-

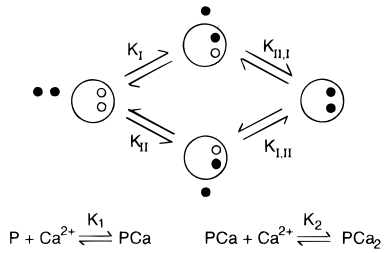

FIGURE 3: Definition of macroscopic (K_1 and K_2) and microscopic (K_I, K_{II}, $K_{I,II}$, and $K_{II,I}$) Ca^{2+}-binding constants.

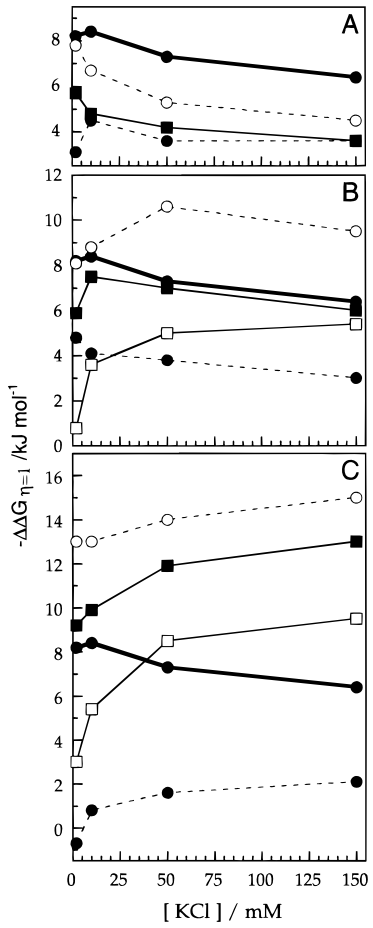

FIGURE 4: Lower limit to the free energy of interaction between the two Ca^{2+} sites, $-\Delta\Delta G_{\eta=1} = RT \ln(4K_2/K_1)$ as a function of salt concentration. The data for the wild-type substitute P43M is shown in all panels (●, solid line). (A) Mutant proteins with substituted residues distant from the Ca^{2+} sites: L6V (■, solid line), V70L (●, dashed line), I73V (○, dashed line). (B) Mutant proteins with substituted residues in the center of the core: F10A (■, solid line), L28A (□, solid line), F66A (○, dashed line), F66W (●, dashed line). (C) Mutant proteins with substituted residues having side chains in the core and involved in the backbone-backbone β-type interaction between the Ca^{2+} sites: L23A (■, solid line), L23G (□, solid line), V61A (●, dashed line), V61G (○, dashed line).

ativity. The values of $-\Delta\Delta G_{\eta=1}$ as a function of salt concentration, are displayed for all mutants in Figure 4, panels A−C. It appears that, for a large fraction of the hydrophobic mutants, $-\Delta\Delta G_{\eta=1}$ is different from the wild-type. The value of $-\Delta\Delta G_{\eta=1}$ decreases with added salt for P43M and for the mutants with substitutions far from the Ca^{2+} sites (Figure 4A). In contrast, $-\Delta\Delta G_{\eta=1}$ increases with added salt for mutants with substitution of β-sheet residues (L23A, L23G, V61A, and V61G, Figure 4C) and other central core residues (L28A and F66A, Figure 4B). As an example, the mutant L28A has much lower value of $-\Delta\Delta G_{\eta=1}$ than P43M at low ionic strength, whereas at 150 mM KCl the values agree within experimental error (Figure 4B).

Ca^{2+} Titrations followed by ^1H NMR. The titrations followed by ^1H NMR show for all mutants a single binding process between zero and 2 equiv of Ca^{2+}, as exemplified in Figure 5 for F66A and L23G. For 10 of the mutants (all but L23G), Ca^{2+} binding is observed to be in the slow-exchange regime on the NMR time scale, i.e., there are several resonances for which the intensity gradually increases or decreases during the course of the Ca^{2+} titration. For L23G, we also observe a small gradual change in chemical shift for a few resonances, suggesting that Ca^{2+} binding to this mutant has entered the intermediate exchange regime. For the 10 mutants with slow exchange behavior, the calcium dissociation rates can be estimated from the maximum NMR line width which occurs at 1 equiv bound Ca^{2+} (*41*). For P43M, L6V, F66W, and I73V there is no observable broadening of the lines during the titration implying that the Ca^{2+} off-rate is lower than 10 s^{-1}. For the mutants L23A, V61G, V61A, F66A and V70L, there is a slight broadening, whereas a more substantial broadening is observed for L28A. The Ca^{2+} off-rate, k_{off}, was estimated from W, the observed maximum line width of backbone amide proton resonances after subtracting the contribution from the scalar NH-C^{α}H coupling as

$$k_{off} = \pi W - 1/T_2 \tag{3}$$

where $1/T_2$ is equal to the natural line width in the absence of exchange. For L23G, the off-rate was estimated using equations pertaining to the intermediate exchange regime (*41*):

$$k_{off} = \frac{\pi\delta\nu^2(W^* + W_0)[1 + 2(W^*/\delta\nu)^2 - (W^*/\delta\nu)^4]^{1/2}}{2(W^{*2} - W_0^{\,2})} \tag{4}$$

where W^* is the maximum line width, W_0 is the line width in the absence of exchange, and $\delta\nu$ is the chemical shift difference between the Ca^{2+}-free and Ca^{2+}-loaded states.

Stopped-Flow Studies of Ca^{2+}-Dissociation Rates. Stopped-flow studies were carried out on all mutants to obtain more accurate values of the Ca^{2+}-dissociation rates. The experiments were repeated at the same four KCl concentrations as the equilibrium calcium titrations to assess the salt dependence of the calcium−calbindin D_{9k} interaction in more detail. A Ca^{2+}-free solution of the chelator quin 2 was mixed with Ca^{2+}-saturated protein. As the reaction of Ca^{2+} with quin 2 is several orders of magnitude faster than the dissociation of Ca^{2+} from the proteins (*42*), the time course of Ca^{2+}-binding to quin 2 can be taken to reflect Ca^{2+} dissociation from the proteins. Data examples are shown in Figure 6, and results are summarized in Table 2.

The Ca^{2+}-dissociation rates, k_{off}, divided the proteins in three groups (Table 2). Two proteins, L6V and I73V, showed a k_{off} which is slightly lower than for P43M. A second and largest group of eight proteins had faster dissociation rates. Five of these, F10A, L23A, V61G, F66A, and V70L, showed a 3−5-fold increase in rate and the three

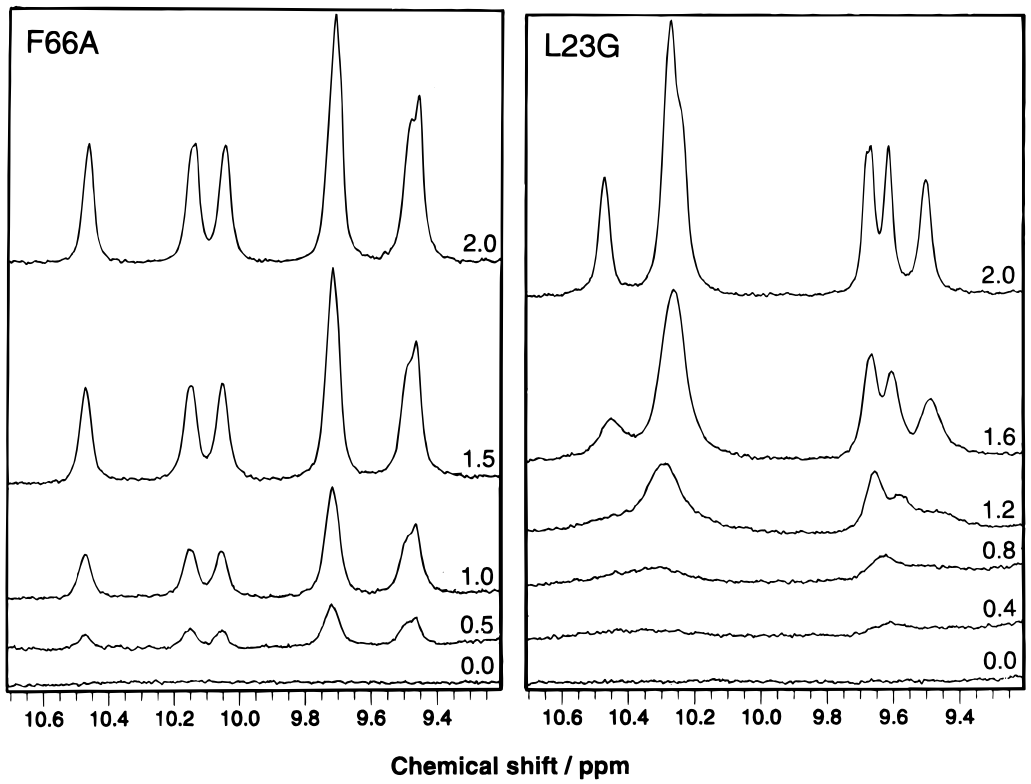

FIGURE 5: ^{1}H NMR spectra recorded during Ca^{2+} titrations of F66A (left) and L23G (right). The amount of calcium in protein equivalents is indicated at each spectrum.

Table 2: Calcium Dissociation Rates, k_{off}, from ^{1}H NMR and Stopped-Flow Experiments

	k_{off}/s^{-1}			
	^{1}H NMR	stopped-flow		
mutant	~50 mM KCl	≤2 mM KCl	salt dependence[a]	salt dep/init rate
wild-type	≤10	4.09 ± 0.04	0.18 ± 0.01	0.044 ± 0.002
P43M	≤10	5.64 ± 0.06	0.26 ± 0.03	0.046 ± 0.005
L6V	≤10	3.11 ± 0.06	0.08 ± 0.01	0.026 ± 0.003
F10A	30 ± 10	28.8 ± 0.7	2.06 ± 0.24	0.071 ± 0.008
L23A	40 ± 20	26.7 ± 0.3	1.74 ± 0.19	0.066 ± 0.007
L23G	140 ± 40	126 ± 7		
L28A	90 ± 40	73 ± 2		
V61A	60 ± 20	50 ± 1		
V61G	20 ± 10	15.0 ± 0.1		
F66A	20 ± 10	10.4 ± 0.1	0.64 ± 0.07	0.062 ± 0.007
F66W	≤10	0.87 ± 0.01	0.028 ± 0.003	0.032 ± 0.003
V70L	40 ± 20	16.5 ± 0.2	0.80 ± 0.17	0.050 ± 0.010
I73V	≤10	3.78 ± 0.03	0.015 ± 0.01	0.040 ± 0.003

[a] Salt dependence = $k_{off}/[KCl]^{1/2}$ (s^{-1} mM^{-1}).

others, L23G, L28A, and V61A, showed more than a 10-fold increase. Only one protein, F66W, had a significantly lower dissociation rate than P43M (Figure 6).

The influence of salt on k_{off} was measured and normalized to the initial off-rate measured at low salt concentration (≤2 mM KCl) to provide a more accurate platform for an analysis of the electrostatic effect of the mutation (Table 2). For the proteins with highest off-rates, it was not possible to measure the rates at higher salt concentration. Two proteins, V70L and I73V, had comparable salt dependence to P43M, two proteins, L6V and F66W, showed a decreased salt dependence, and finally, three proteins, F10A, L23A, and F66A, had off-rates more sensitive to the electrostatic environment. Examples are shown in Figure 6.

Conformation and Dynamics from 2D ^{1}H NMR. All mutants were studied using one-dimensional NMR, and their spectra were highly similar to that of P43M, with the possible exception of L23G. The F66A mutant was studied in more detail using two-dimensional NMR and was found to have retained the structure of the wild-type protein (B.E.F, unpublished result). As part of the effort to determine the molecular basis for the perturbations of Ca^{2+}-binding properties in the hydrophobic core mutants, structural and dynamic properties of both the apo and Ca^{2+}-bound states of V61A have been examined by 2D ^{1}H NMR and compared to P43M. Complete resonance assignments were obtained using a backbone-based assignment strategy (*43*). The backbone NH and $C^{\alpha}H$ chemical shifts are compared to those of P43M in Figure 7. There is a slightly greater number of statistically significant differences in chemical shifts in the Ca^{2+}-loaded state as opposed to the apo state. However, most differences are barely outside of the experimental error and can be attributed to the inability to make the experimental conditions exactly identical. Substantial differences in the backbone proton chemical shifts (>0.1 ppm) are observed only in close spatial proximity of the mutation. The general similarity in chemical shifts also extends to side-chain proton resonances, even those that have substantial ring-current shifts and are, therefore, very sensitive probes of structural similarity. For example, the highest upfield-shifted methyl group, Val70 $C^{\gamma}H$ in the apo state and Ile73 $C^{\delta}H$ in the Ca^{2+}-loaded state, has a chemical shift that is nearly identical to that of the wild-type protein.

We have also examined a large number of characteristic NOEs, especially those critical to the definition of the elements of secondary structure and the global folding pattern that have been discussed previously (*44*). Most significantly,

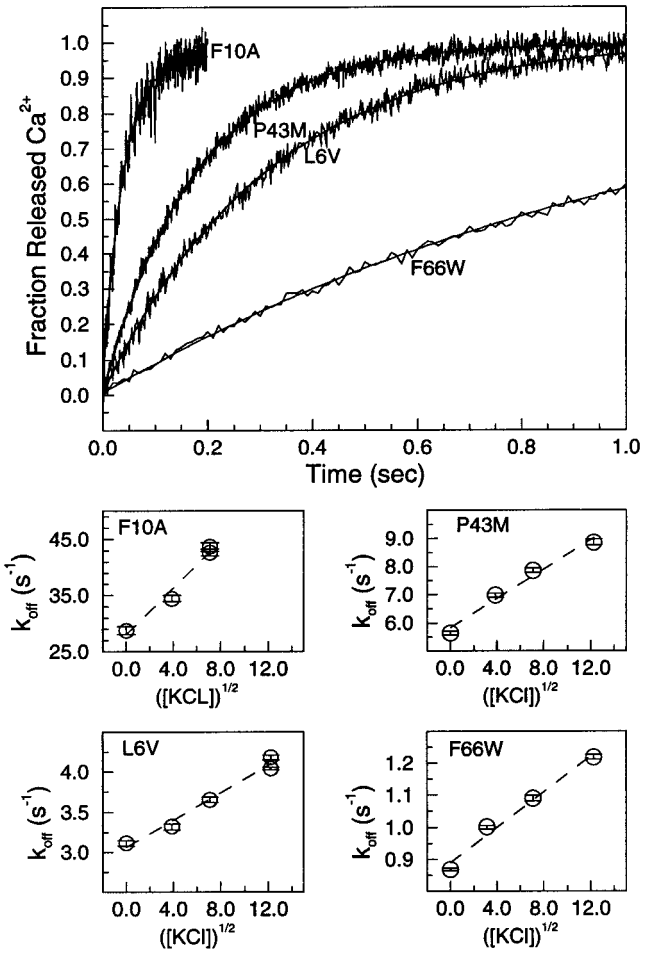

FIGURE 6: Stopped-flow fluorescence kinetic traces for L6V, F10A, P43M, and F66W together with fitted curves using single-exponential functions plus a linear correction for photobleaching. Below is shown the salt dependence of the Ca^{2+} dissociation rate constants for the same four proteins.

in the vicinity of the mutation, i.e., in the region near the hydrogen bonds that cross between the two binding loops, we find that in the apo state certain of the cross-strand NOEs are absent or significantly weaker than in the wild-type protein. The following NOEs are present in apo P43M, but absent in apo V61A: $d_{\alpha\alpha}(22,62)$; $d_{\alpha N}(22,63)$; $d_{\alpha N}(62,63)$; d_{NN}-(23,62). On the other hand, $d_{\alpha N}(22,23)$ and $d_{NN}(23,61)$ are present in both P43M and V61A, whereas $d_{\alpha N}$ (60,61) and $d_{\alpha\alpha}(24,60)$ are overlapped and not assignable in V61A. The combination of those NOEs that are observed and low amide proton exchange rates for Ala61 and Leu23 indicate that the two key cross-strand hydrogen bonds are still intact. The NOE data do however suggest that this interaction may be somewhat weaker than in the wild-type protein. The extensive similarity of virtually all backbone and side-chain methyl/aromatic proton chemical shifts, as well as nearly all characteristic NOEs, indicates that the apo state of V61A is otherwise very similar to the that of the wild-type protein.

In contrast to the apo state, we find that the characteristic NOEs of the Ca^{2+}-loaded state are virtually identical to P43M. At the semiquantitative level of analysis, the amide proton exchange rates are also found to be similar. As an additional probe of the internal dynamics, the line widths of the aromatic ring proton resonances of Phe10 have been examined in both 1D and 2D spectra. In the wild-type and other mutant proteins, these resonances are exchange broadened in the Ca^{2+}-loaded state, an effect attributed to slowed rates of 180° ring flips associated with a more compact and stable packing of hydrophobic side chains in the protein core. The line widths of these resonances in $(Ca^{2+})_2$-V61A are found to be the same as those of the wild-type protein. Overall, the observed similarity of the structural and dynamic probes supports the conclusion that the Ca^{2+}-bound state of the V61A mutant is effectively identical to the wild-type protein, except for very minimal and highly localized perturbations in the vicinity of the mutation. Thus, although the number of backbone chemical shifts that are perturbed is greater than for the apo state, there is no indication of possible perturbation of the cross-strand hydrogen-bonding interaction between the two binding loops as was detected for the apo state.

DISCUSSION

It is evident from the present results that interactions within the hydrophobic core do affect the ligand-binding properties of a protein, even in the absence of direct contacts between the core residues and the ligand. Each of the calbindin D_{9k} mutants studied here has an altered side-chain volume of a single hydrophobic core residue, and for eight of them, we

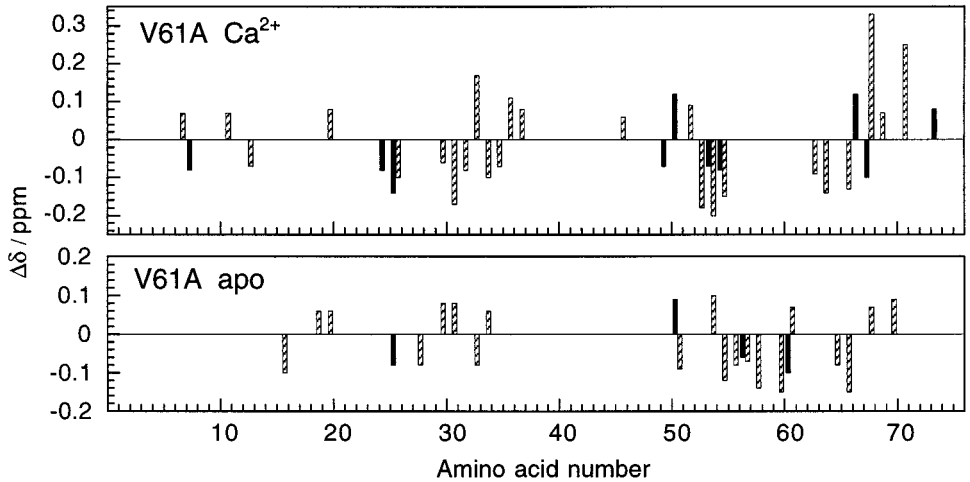

FIGURE 7: Comparison of backbone chemical shifts of V61A and P43M, represented as $\Delta\delta = \delta(\text{V61A}) - \delta(\text{P43M})$. All $\Delta\delta$ values are ≥ 0.06 ppm are shown. Filled bars represent α-protons and crosshatched bars NH protons. The Ca^{2+}-bound states are compared in the upper panel and the apo states in the lower panel.

observe a reduced Ca^{2+} affinity and increased Ca^{2+}-dissociation rate. The replacement of the core residues Phe10, Leu28, Val61, Phe66, and particularly Leu23 with alanine or glycine leads to large reductions in Ca^{2+} affinity and substantial increases in Ca^{2+}-dissociation rate. It is probably not surprising that the largest perturbations occur for the mutant L23G, with the complete removal of a bulky hydrophobic side chain of a core residue whose backbone is part of one of the calcium-binding loops and involved in important stabilizing interactions with the adjacent site. For L23G, the overall affinity of binding two calcium ions, K_1K_2, has decreased by a factor of 1700 ($\delta\Delta G_{tot} = 19$ kJ mol^{-1}). A plot of the mutational effect on calcium affinity versus distance of mutated side chain to the nearest calcium coordinating atom, reveals a significant correlation ($R = 0.77$, graph not shown). Only small changes in the affinities and off-rates are observed for L6V, V70L, and I73V, in which the substituted residues are located far from the Ca^{2+} sites. The mutations Leu6 → Val, Val70 → Ile and Ile73 → Val lead to rather small volume changes, so the lack of substantial effects is hardly surprising for these mutants. The effects (up to a factor of 3) are nevertheless nonnegligible and corroborate earlier findings that the Ca^{2+}-binding properties can be modulated by substitutions at the opposite end of the protein with respect to the binding sites (Groves et al., 1997).

The increase in Ca^{2+} affinity observed for F66W is quite remarkable. The overall affinity of binding two calcium ions, K_1K_2, has increased by a factor of 25 ($\delta\Delta G_{tot} = -8$ kJ mol^{-1}). It is the largest increase in affinity observed for any mutant of calbindin D_{9k} among the 73 produced this far, and it illustrates that the configuration of the core in the wild-type is not optimized to yield the highest possible Ca^{2+} affinity. One may assume that a significant increase in affinity would be detrimental to the biological function of calbindin D_{9k}. It is important for both the buffering and regulatory Ca^{2+}-binding proteins to have affinity as well as on- and off-rates fine-tuned to meet the requirements imposed by the environmental Ca^{2+} levels. Very few Ca^{2+}-related functions can be served by a protein that is always in the Ca^{2+}-bound state.

Correlation Between Ca^{2+} Affinity and Dissociation Rate. For the 11 calbindin D_{9k} mutants studied in the present work, there is a significant correlation between the Ca^{2+}-dissociation rate as measured by stopped-flow fluorescence and the Ca^{2+} affinity as measured from equilibrium competition experiments ($R = 0.94$; Figure 8). This suggests that the variation in affinity among the hydrophobic core mutants is a consequence of perturbations of the off-rate. In contrast, for a series of mutants with charge substitutions on the protein surface, effects on the on-rate were responsible for the affinity changes (*45*). From the values of k_{off} and K_2 we can estimate the on-rate of the second bound Ca^{2+}-ion as $k_{on} = K_2k_{off}$. This yields association rate constants ranging from 4×10^8 to 2×10^9 M^{-1}s^{-1}. Thus, the variation in on-rate is within a factor of 5. This is a fairly small interval compared to the large spread of dissociation rates (within a factor of 150).

Correlation between Ca^{2+} Affinity and Apo Protein Stability. The free-energy changes in the present and previous paper in this issue (*1*) relate different states to the folded apo state (Figure 9). The quantity measured in the previous paper in this issue, ΔG_{NU}(apo), is the free energy change on going from the folded apo protein to the denatured state. A

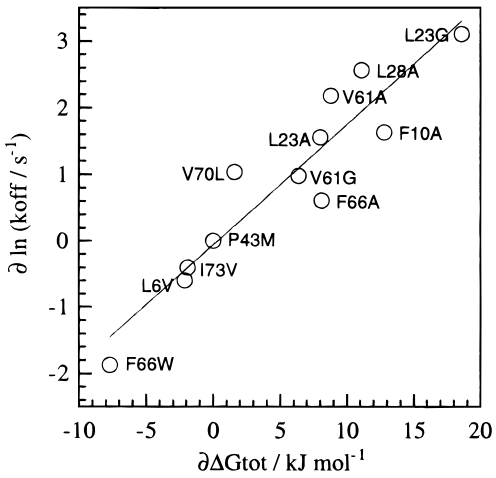

FIGURE 8: Correlation of mutational effects on the Ca^{2+}-dissociation rate, k_{off}, as measured by stopped flow fluorescence and on the total affinity of binding two Ca^{2+} ions, ΔG_{tot}, as measured from titrations in the presence of quin 2 or 5,5′-Br_2BAPTA. The solid line was obtained by linear least-squares fitting to the data. The correlation coefficients is 0.94.

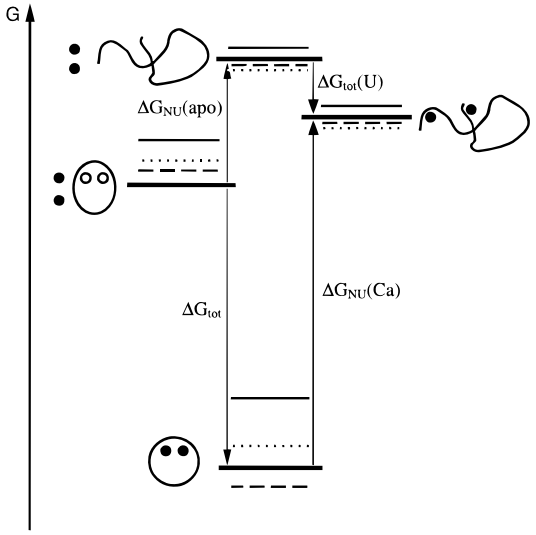

FIGURE 9: Thermodynamic cycle. The thick solid lines depict the free energy of P43M in apo and Ca^{2+} form as well as the denatured form with and without Ca^{2+}-bound. The thins solid lines represent a mutant with decreased Ca^{2+} affinity (ΔG_{tot}), decreased stability of the apo form, and even more decreased stability of the Ca^{2+} form. The dotted lines represent a mutant with slightly increased Ca^{2+} affinity (ΔG_{tot}), decreased stability of both the apo form and the Ca^{2+} form. The dashed lines represent a mutant with increased Ca^{2+} affinity (ΔG_{tot}), decreased stability of the apo form and increased stability of the Ca^{2+} form.

mutational effect on the stability is thus a function of perturbations of the folded and unfolded apo state. On the contrary, an effect on the Ca^{2+} affinity is caused by differences in the perturbations of the apo and Ca^{2+}-bound states, because the total free-energy change on calcium binding, ΔG_{tot}, compares the Ca^{2+} state to the apo state plus two solvated ("free") Ca^{2+} ions. For all mutants in the present study, the value of ΔG_{tot} is negative and the value of ΔG_{NU}(apo) is positive. In Figure 10A, the effect of each mutation on ΔG_{NU}(apo) is compared to the effect on ΔG_{tot}. [$\delta\Delta G_{NU}$(apo) = $\Delta G_{NU}(\text{apo})_{mutant} - \Delta G_{NU}(\text{apo})_{P43M}$, and $\delta\Delta G_{tot} = \Delta G_{tot,mutant} - \Delta G_{tot,P43M}$]. There is a correlation between the two quantities ($R = 0.69$), suggesting that one mechanism by which the hydrophobic core residues enhance

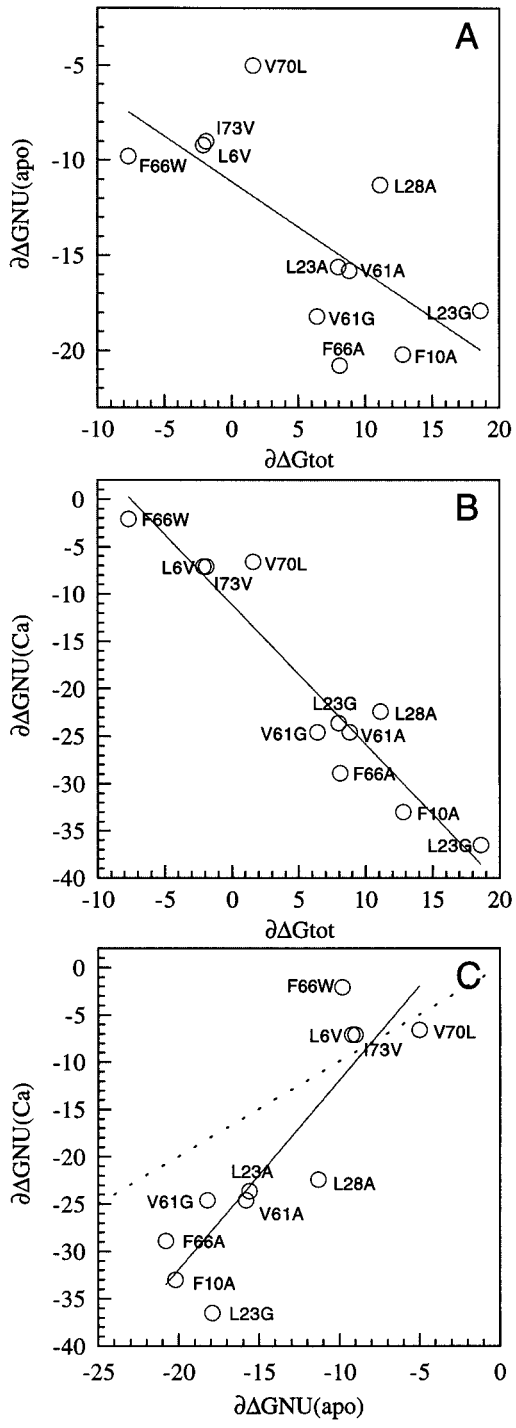

FIGURE 10: Comparison of the effect of each mutation on the total affinity of binding two Ca^{2+} ions, ΔG_{tot}, and on stability, ΔG_{NU}. (A) $\delta\Delta G_{tot}$ versus $\delta\Delta G_{NU}$(apo), (B) $\delta\Delta G_{tot}$ versus $\delta\Delta G_{NU}$(Ca), and (C) $\delta\Delta G_{NU}$(Ca) versus $\delta\Delta G_{NU}$(apo). The solid lines were obtained by linear least-squares fitting to the data. The correlation coefficients were 0.69, 0.95, and 0.89 in panels A, B, and C, respectively. $\delta\Delta G_{NU}(apo) = \Delta G_{NU(apo),mutant} - \Delta G_{NU(apo),P43M}$, and $\delta\Delta G_{tot} = \Delta G_{tot,mutant} - \Delta G_{tot,P43M}$.

calcium affinity is by contributing to the preformation of the binding sites in the apo state. This is in analogy to the macrocycle effect observed for small chelates. The low value of R underscores that the two quantities are not controlled entirely by the same factors. For example, the F66A mutation leads to the largest reduction in stability toward urea denaturation of the apo state, but there are several mutants with lower Ca^{2+} affinity.

Correlation between Ca^{2+} Affinity and Stability of the Ca^{2+}-Bound State. With measurements of both the free energy of Ca^{2+} binding and the free energy of unfolding of the apo state we may calculate the effect of each substitution on the free energy of unfolding of the calcium state. These calculations rely on the assumption that the denatured states of P43M and all mutants bind Ca^{2+} with the same (low) affinity (Figure 9). The assumption seems reasonable as in the denatured state Ca^{2+} interacts weakly with carboxylate groups on the unfolded chain, and the nature of the hydrophobic groups probably has very little effect on this interaction. The effect on the stability toward denaturation of the Ca^{2+} state, $\partial\Delta G_{NU}$(Ca), can then be calculated as $\delta\Delta G_{NU}(Ca) = \delta\Delta G_{NU}(apo) - \delta\Delta G_{tot}$. There is a strong correlation between this quantity and the effect on calcium affinity ($R = 0.95$, Figure 10B), suggesting that the main mechanism by which the hydrophobic core residues promote high Ca^{2+} affinity is by preferential stabilization of the Ca^{2+}-bound form. This goes well in hand with the dissociation rates, which reflect perturbations of the Ca^{2+}-bound state, being more affected than the association rates. We cannot calculate the absolute value of the stability of the Ca^{2+} state of wild-type nor any mutant as long as the free energy of Ca^{2+}-binding to denatured calbindin D_{9k} is unknown.

A change in Ca^{2+} affinity can be achieved by different combinations of effects on free energies of the free and bound states. Three situations would lead to a reduced calcium affinity: (1) the mutation increases the free energy of the Ca^{2+}-bound state more than that of the apo state (i.e., the Ca^{2+} state is most destabilized), (2) the mutation decreases the free energy of the apo form more than that of the Ca^{2+}-bound form (i.e., the apo state is most stabilized), or (3) the Ca^{2+}-bound state is destabilized and the apo state is stabilized. Situation (1) seems to hold for all hydrophobic core mutants with reduced Ca^{2+} affinity: F10A, L23A, L23G, L28A, V61A, V61G, F66A, and V70L [they are found below the dashed line drawn for $\delta\Delta G_{NU}(Ca) = \delta\Delta G_{NU}(apo)$ in Figure 10C]. Situation 1 can also be attributed to better tolerance of the mutation in the apo state, which we believe is the result of greater intrinsic flexibility and intrinsically lower stability of the apo protein. Supporting evidence comes from reconstitution experiments with two fragments comprising the N- and C-terminal EF-hands which have pointed to a more specific packing of the core in the Ca^{2+}-bound state (*22*). Both NH exchange and ^{15}N relaxation studies indicate higher rates of internal fluctuations in the apo state (*46*−*48*).

Cooperativity of Calcium Binding. The chelator method yields macroscopic Ca^{2+}-binding constants and thus provides only a lower limit to the cooperativity, $-\Delta\Delta G_{\eta=1}$. Perturbations of this parameter need not necessarily reflect altered cooperativity. Changes in relative affinities, K_{II}/K_I, for the two sites will also affect the value of $-\Delta\Delta G_{\eta=1}$. For example, a change in relative affinities from 1 to 10 gives a contribution of 2.7 kJ/mol meaning that $-\Delta\Delta G = -\Delta\Delta G_{\eta=1} + 2.7$, i.e., the magnitude of the cooperativity is underestimated by 2.7 kJ/mol. For the wild-type, K_{II}/K_I is close to unity (*12*). Therefore, an increase in $-\Delta\Delta G_{\eta=1}$, must reflect an increase in the cooperativity. This holds at all salt concentrations for mutants F66A, L23A, and V61G, and at high salt for L23G. For mutants with a slightly reduced value of $-\Delta\Delta G_{\eta=1}$, we cannot exclude that the sites are

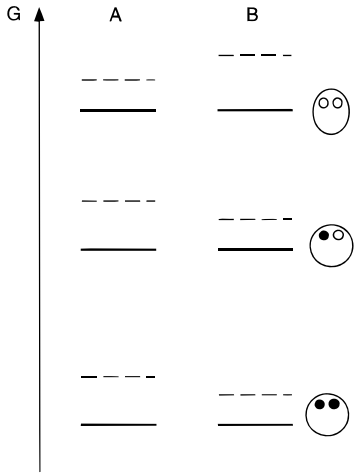

FIGURE 11: Schematic free energy diagram of wild-type and two mutants with (A) increased and (B) decreased cooperativity. The diagram is simplified and shows only one-half saturated state.

perturbed to different extents instead of the cooperativity being decreased. This pertains to I73V, and maybe also L6V, V70L, and F66W, although it seems unlikely that remote mutations giving small effects on overall affinity, K_1K_2, would perturb the two sites very differently. We believe the large reduction in $-\Delta\Delta G_{\eta=1}$ observed for V61A at low salt reflects a decreased cooperativity. Otherwise, a more than a 100-fold difference in the affinities for the two sites is needed to explain the results.

The substantial increase in cooperativity observed for L23A, L23G, V61G, and F66A contrasts the observations on most other types of mutants as does the increase in cooperativity with added salt. An explanation may be derived by considering the mutational effects on three forms of the protein, the apo, the half-saturated, and the Ca^{2+}-loaded form. Detailed structural studies of half-saturated states of calbindin D_{9k}(44,49) have revealed that their structure, including the detailed packing of the hydrophobic core, is much closer to the Ca^{2+}-saturated protein than to the apo form. We may then assume that the mutational effects on the stability of the half-saturated states parallel those of the fully Ca^{2+}-bound state. For mutants with larger reduction in stability of the Ca^{2+} state compared to the apo state (below the dashed line in Figure 10C) we would then have a situation as sketched in Figure 11A, and the affinity for the first bound ion would be more reduced than the affinity for the second ion, leading to increased cooperativity. This is indeed the case for L23A, L23G, V61G, and F66A. The opposite case, mutants with a smaller reduction of the stability of the calcium state than of the apo state (above the dashed line in Figure 10C) would face a situation as in Figure 11B, with an increase in the affinity for the first bound ion and the affinity for the second step retained. In that situation, we would have increased affinity and decreased cooperativity, as is indeed found for F66W and probably also for L6V. The effects would be more pronounced at higher salt concentrations, reconciling the salt-induced increase in cooperativity for L23A, L23G, V61G, F66A, F10A, L28A, and V61A, as well as the salt-induced decrease observed for F66W ad L6V. Thus, a more optimized core packing of the Ca^{2+}-loaded state could be detrimental to the function, both by increasing the Ca^{2+} affinity and by impeding the positive cooperativity.

Structural Effects of Mutations. The V61A mutant was chosen for an in-depth ^{1}H NMR analysis for several reasons. It falls in the group of mutants in which large effects are seen on stability and calcium affinity, as well as calcium dissociation rates, but it is not the most extremely perturbed in any of these respects. It lies close to the fitted line in all the correlation plots (Figures 8 and 10, panels A−C) and is presumed to be a good representative for the group. More specifically it is a representative for mutants with substitutions of the two β-sheet residues. Another reason for choosing V61A was the large effect on the cooperativity of calcium binding observed for this mutant. The detailed ^{1}H NMR analysis of V61A shows that there is only very limited perturbation of the structure of the protein upon removal of one of these hydrophobic side chains. The only detectable effect on the structural and dynamical properties of the mutant relative to wild-type is in the strength of the cross-strand hydrogen bonds between the two binding loops, based on the pattern of NOEs. This shows that the mutational effects on the binding properties can be reasonably large without any *long-range* effects on protein structure and dynamics.

A similar conclusion can be drawn for the other mutants, albeit somewhat less directly, based on the very great similarity of their NMR spectra with that of P43M and V61A proteins.

Cross-Strand Interaction between the Ca^{2+} Sites. The short β-type interaction between the two calcium loops, involving mainly residues Val61 and Leu23, has been suggested to play a role in the cooperativity of Ca^{2+} binding (*50*). However, with this being a backbone−backbone interaction, it is difficult to probe by mutagenesis. The substitution of alanine or glycine for Val61 or Leu23 does not appear to abolish the hydrogen bonds between the loops, although large hydrophobic residues are found in the corresponding positions in most EF-hand pair domains, with their side chains below the Ca^{2+}-binding loops buried in the hydrophobic core. The mutations involving residues 23 and 61 do, however, lead to large reductions in affinity, and the results for L23A and L23G conform to our expectations with the effect of the Leu → Ala substitution being somewhat smaller than for the Leu → Gly substitution. The effects of the corresponding mutations in position 61 are more surprising in that V61G binds Ca^{2+} with higher total affinity than V61A. Furthermore, the cooperativity of ion binding, which was reduced in the V61A mutant, is more than regained in V61G. In fact, V61G has higher cooperativity than the wild-type protein! The result for V61A alone (a very low level of cooperativity) would suggest either that the Val61 side chain has a direct role in transmitting the cooperativity, or that the observed reduction is a secondary effect due to a perturbation of other structural elements (for example, charged groups in the calcium-binding loops) that are involved in the cooperative mechanism. However, the high cooperativity observed for the V61G mutant rules out the possibility that the Val61 side chain is crucial, but suggests that instead, it is the detailed conformation in the loop region which is important and perturbed to different extents in V61A and V61G. This conclusion is corroborated by our results for L23A and L23G showing that the Leu23 side chain is not crucial for the positive cooperativity and that the details of loop configuration comes into play. A significant

Table 3: Solvent Accessible Surface Area of Hydrophobic Side Chains in Calbindin D_{9k}

	solvent accessible surface area[a]/Å^2		
side chain	Apo (1clb)	Ca^{2+} (2bda)	free[b]
Leu6	14 ± 11	27 ± 12	170
Phe10	1 ± 1	3 ± 2	210
Leu23	0	0	210
Leu28	2 ± 2	1 ± 1	210
Val61	1 ± 1	0	155
Phe66	1 ± 1	1 ± 1	210
Val70	13 ± 8	25 ± 5	155
Ile73	49 ± 15	35 ± 12	175

[a] The total side-chain accessible surface areas were calculated for two states of NMR solution structures, 1clb (apo) and 2bca (Ca^{2+}), using the program naccess (*51*). The values are the mean of 33 and 32 structures, respectively. [b] Values for the free amino acids are taken from ref *52* and represent the entire residue.

contribution to the positive cooperativity from the spatial distribution of charges around the Ca^{2+} sites has also been deduced using the mutants E17Q, D19N, E60Q, and E60D (*12*, *51*). The results for E60D are especially intriguing showing a significant enhancement of the cooperativity in a mutant with a small translation of one negative charge (*51*).

The mutants L23A and V61A may also suffer from having the strong helix-promoting amino acid alanine in positions that are in β-conformation. Compared to valine and leucine, alanine destabilizes a β-sheet by 3.4 and 2.1 kJ mol^{-1}, respectively (*52*). If this effect is more pronounced in the Ca^{2+} state, which has a more rigid β-type interaction, this will contribute to the reduction in Ca^{2+} affinity seen for these mutants. Glycine is, in general, more destabilizing than alanine (by 4.6 kJ mol^{-1}; ref *52*), which could explain part of the difference between L23G and L23A. On the other hand, the difference between V61G and V61A, goes in the other direction. Although the destabilization of a β-sheet by glycine relative to alanine is context dependent, it seems less far-fetched to believe the explanation is to be found in other effects (e.g., redistribution of charged groups in the loop region).

Relation between Solvent-Accessible Surface Area and Mutational Effect. The mutational effects on calcium affinities appear in some cases to be related to changes in solvent-accessible surface area (SASA) on calcium binding. The SASA for the substituted residues in the solution structures of apo (*28*) and Ca^{2+}-loaded (*27*) calbindin D_{9k} are listed in Table 3. Apparently, several of the substituted residues, Phe10, Leu23, Leu28, Val61, and Phe66, are completely buried in both states. It is for the mutations of these five residues that the by far largest effects on affinity and dissociation rates are observed. The remaining three residues, Leu6, Val70, and Ile73 are partly exposed to solvent. Leu6 has a solvent accessible surface area that increase from 14 to 27 Å^2 when going from apo to Ca^{2+}-loaded protein. A smaller side chain in position 6 may promote higher calcium affinity, which is indeed observed for the mutant L6V. For Val70 there is a significant increase in SASA on Ca^{2+} binding. A larger side-chain as in the mutant V70L is thus more unfavorable and may explain the observed reduction in Ca^{2+} affinity.

Salt Effects on Dissociation Rates and Cooperativity. The salt dependence on calcium dissociation rates are strongly correlated to the distance to the nearest calcium coordinating atom ($R = 0.97$), Figure 12. The closer the residue is to the nearest calcium-coordinating atom, the higher the salt dependence introduced by the mutation. An increased salt dependence of the dissociation rates is thus seen for F10A, L23A, and F66A and is possibly the case also for L23G and L28A. For the mutants with truncation performed far away from the calcium-coordinating atoms, a decreased salt dependence is observed. Calculation of on-rates as above suggests that the salt dependence on the on-rate is very similar to that of P43M.

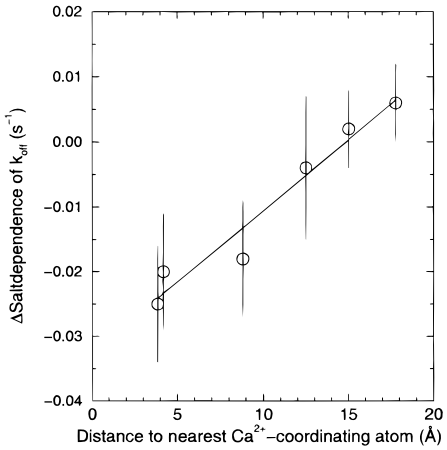

FIGURE 12: Correlation of salt dependence of Ca^{2+}-dissociation rates and the distance from mutated side chain to the nearest Ca^{2+}-coordination atom.

Interestingly, the cooperativity of calcium binding increases in response to added salt for the same group of mutants that display increased salt dependence of the dissociation rates. For F66W, both a decreased salt dependence of the dissociation rate as compared to the wild-type (P43M) and a decreased cooperativity are observed. The same is true for L6V, showing that the affinity promoting effects of the substitution Leu6 → Val and Phe66 → Trp are even higher at higher salt concentration. In all cases, the stabilization of the calcium-bound state may be the key factor in determining the calcium-binding properties. Increased salt concentrations make the hydrophobic interactions more important and induces a larger spread among the mutants. The hydrophobic core residues of a calcium-binding protein may thus be important not only for stabilizing the hydrophobic core, but also for the preformation and continuous structural stabilization of the Ca^{2+}-binding sites.

CONCLUSION

Although many binding events occur at specific sites in a protein, binding properties of globular proteins are critically dependent on the structural integrity of the hydrophobic core. We have observed substantial effects on Ca^{2+} affinity and dissociation rates in calbindin D_{9k} due to large volume changes in the central parts of the core. Analysis of a large set of similar substitutions spread over the protein molecule was of great advantage for the interpretation of our results. These show that long-range effects cannot be neglected when discussing factors that govern affinity and dissociation rates in Ca^{2+}-binding proteins. These effects are likely mediated through an altered probability of the correctly folded form that contains the binding site. That is, the hydrophobic core residues promote Ca^{2+} binding by contributing to preforma-

tion of the sites in the apo state. An even larger contribution to the Ca^{2+} affinity comes from preferential stabilization of the Ca^{2+}-bound state. The effects from distant substitutions are small but significant, showing that the Ca^{2+}-binding properties are functions of the entire protein molecule, and can be fine-tuned even by adjustments at the opposite end of the protein with respect to the calcium-binding sites. The combined results demonstrate that the mutational effects on the binding properties can be reasonably large without any long-range effects on protein structure and dynamics.

ACKNOWLEDGMENT

We thank Karin Julenius and Sture Forsén for critically reading the manuscript and Eva Thulin for the mutant proteins.

REFERENCES

1. Julenius, K., Thulin, E., Linse, S., and Finn, B. E. (1998) *Biochemistry 37*, 8915−8925.
2. Haiech, J., Kilhoffer, M. C., Lukas, T. J., Craig, T. A., Roberts, D. M., and Watterson, D. M. (1991) *J. Biol. Chem. 266*, 3427−3431.5; Falke, J. J., Drake, S. K., Hazard, A. L., and Peersen, O. B. (1994) *Q. Rev. Biophys. 27*, 219−290.
3. Babu, A., Su, H., Ryu, Y., and Gulati, J. (1992) *J. Biol. Chem. 227*, 15469−15474.
4. Wu, X., & Reid, R. E. (1997) *Biochemistry 36*, 8649−8656.
5. Linse, S., and Forsén, S. (1995) *Adv. Second Messenger Phospoprotein Res. 30*, 89−151.
6. Falke, J. J., Drake, S. K., Hazard, A. L., and Peersen, O. B. (1994) *Q. Rev. Biophys. 27*, 219−290.
7. Pearlstone, J. R., McCubbin, W. D., Kay, C. M., Sykes, B. D., and Smillie, L. B. (1992) *Biochemistry 31*, 9703−9708.
8. Trigo-Gonzales, G., Awang, G., Racher, K., Neden, K., and Borgford, T. (1993) *Biochemistry 32*, 9826−9831.
9. Grabarek, Z., Tan, R. Y., Wang, J., Tau, T., and Gergerly, J. (1990) *Nature 345*, 132−135.
10. Grabarek, Z., Tan, R. Y., and Head J. (1991) *Biophys. J. 59*, 23a.
11. Linse, S., Brodin, P., Johansson, C., Grundström, T., Drakenberg, T., and Forsén, S. (1988) *Nature 335*, 651−652.
12. Linse, S., Johansson, C., Brodin, P., Grundström, T., Drakenberg, T., and Forsén, S. (1991) *Biochemistry 30*, 154−162.
13. Svensson, B., Jönsson, B., Woodward, C. E., and Linse, S. (1992) *Biochemistry 30*, 5209−5217.
14. Buchanan, J. D., Corbett, R. J. T., and Roche, R. S. (1986) *Biophys. Chem. 23*, 183−199.
15. Hamano, M., Nitta, K., Kuwajima, K. and Sugi, S. (1986) *J. Biochem. 100*, 1617−1622.
16. Kesvatera, T., Jönsson, B., Thulin, E., and Linse, S. (1994) *Biochemistry 33*, 14170−14176.
17. Linse, S., Jönson, B., and Chazin, W. J. (1995) *Proc. Natl. Acad. Sci. U.S.A.* 92, 4748−4752.
18. Shaw, G. S., Hodges, R. S., and Sykes, B. D. (1990) *Science 249*, 280−283.
19. Shaw, G. S., Findlay, W. A., Semchuk, P. D., Hodges, R., and Sykes, B. D. (1992) *J. Am. Chem. Soc. 114*, 6258−6259.
20. Reid, R. E. (1990) *J. Biol. Chem. 265*, 5971−5976.
21. Finn, B. E., Kördel, J., Thulin, E., Sellers, P., and Forsén, S. (1992) *FEBS Lett. 298*, 211−214.
22. Linse, S., Thulin, E., and Sellers, P. (1993) *Protein Sci. 2*, 985−1000.
23. Permyakov, E. A., Medvekin, V. N., Mitin, Y. V., and Kretsinger, R. H. (1991) *Biochim. Biophys. Acta 1976*, 67−70.
24. Durussel, I., Luan-Rilliet, Y., Petrova, T., Takagi, T., and Cox, J. A. (1993) *Biochemistry 32*, 2394−2400.
25. Szebenyi, D. M. E., and Moffat, K. (1986) *J. Biol. Chem. 261*, 8761−8777.
26. Svensson, L. A., Thulin, E., and Forsén, S. (1992) *J. Mol. Biol. 223*, 601−606.
27. Kördel, J., Skelton, N. J., Akke, M., and Chazin, W. J. (1993) *J. Mol. Biol. 231*, 711−734.
28. Skelton, N. J., Kördel, J., and Chazin, W. J. (1995) *J. Mol. Biol. 249*, 441−462.
29. Skelton, N. J., Kördel, J., Akke, M., Forsén, S., and Chazin, W. J. (1994) *Nat. Struct. Biol. 1*, 239−245.
30. Johansson, C., Brodin, P., Grundström, T., Thulin, E., Forsén, S., and Drakenberg, T. (1990) *Eur. J. Biochem. 187*, 455−460.
31. Aue, W. P., Bartholdi, E., and Ernst, R. R. (1976) *J. Chem. Phys. 64*, 2229−2246.
32. Braunschweiler, L., and Ernst, R. R. (1983) *J. Magn. Reson. 53*, 521−528.
33. Macura, S., and Ernst, R. R. (1980) *Mol. Phys. 41*, 95−117.
34. Levitt, M., and Freeman, H. (1979) *J. Magn. Reson. 33*, 473−476.
35. Shaka, A. J., Lee, C. J., and Pines, A. (1988) *J. Magn. Reson. 77*, 274−293.
36. Rance, M. (1987) *J. Magn. Reson. 74*, 557−564.
37. Otting, G., Widmer, H., Wagner, G., and Wüthrich, K. (1986) *J. Magn. Reson. 66*, 187−193.
38. Rance, M., and Byrd, R. A. (1983) *J. Magn. Reson. 54*, 221−240.
39. Davis, D. G. (1989) *J. Magn. Reson. 81*, 603−607.
40. Chazin, W. J., Kördel, J., Drakenberg, T., Thulin, E., Brodin, P., Grundström, T., and Forsén, S. (1989) *Proc. Natl. Acad. Sci. U.S.A. 86*, 2195−2199.
41. Sandström, J. (1982) *Dynamic NMR spectroscopy*, London, Academic Press.
42. Martin S. R., Andersson-Teleman A., Bayley P. M., Drakenberg T., and Forsén, S. (1985) *Eur. J. Biochem. 151*, 543−550.
43. Wütrich, K. (1986) *NMR of Proteins and Nucleic Acids*.
44. Wimberly, B., Thulin, E., and Chazin, W. J. (1995) *Protein Sci. 4*, 1045−1055.
45. Martin, S. R., Linse, S., Johansson, C., Bayley, P. M., and Forsén, S. (1990) *Biochemistry 29*, 4188−4193.
46. Linse, S., Teleman, O., and Drakenberg, T. (1990) *Biochemistry 29*, 5925−5934.
47. Skelton, N. J., Kördel, J., Akke, M., and Chazin, W. J. (1992) *J. Mol. Biol 0.227*, 1100−1117.
48. Akke, M., Skelton, N. J., Kördel, J., Palmer, A. G., and Chazin, W. J. (1993) *Biochemistry 32*, 9832−9844.
49. Akke, M., Forsén, S., and Chazin, W. J. (1995) *J. Mol. Biol. 252*, 102−121.
50. Wesolowski, T. A., Bohuta, G., and Bierzynski, A. (1990) *Protein Eng. 4*, 121−124.
51. Linse, S., Bylsma, N. R., Drakenberg, T., Sellers, S., Forsén, S., Thulin, E., Svensson, L. A., Zajtzeva, I., Zajtzev, V., and Marek, J. (1994) *Biochemistry 33*, 12478−12486.
52. Minor, D. L., and Kim, P. S. (1994) *Nature 367*, 660−663.
53. Hubbard, S. J., and Thornton, J. M. (1993) NACCESS Computer Program, Department of Biochemistry and Molecular Biology, University College of London).
54. Chothia, J. (1975) *J. Mol. Biol. 105*, 1−14.

BI9726436